ORIGINAL ARTICLE

lajss.org© Latin American Journal of Solids and Structures

www.lajss.org

Performance evaluation of a new anchorage system for unbonded post-tensioned GFRP concrete beams

Luana Ferreira Borges[a*], **Rodrigo de Melo Lameiras**[a]

[a] Department of Civil and Environmental Engineering, University of Brasília, Brasília, Brazil. Email: luana_f.borges@hotmail.com, rmlameiras@unb.br

* Corresponding author

https://doi.org/10.1590/1679-7825/e9006

Abstract

Conventional steel strand anchorages are unsuitable for fiber-reinforced polymer (FRP) materials. This study evaluates a new bond-type anchorage system for unbonded post-tensioned GFRP bars. Prestressing is applied through a steel strand housed within a component threaded onto an adapter connected to the live-end anchorage. Two concrete beams reinforced with two post-tensioned GFRP bars were tested. The bars in Beam 1 were prestressed to 45.1% of their guaranteed tensile strength, and those in Beam 2 to 27.5%. Concrete strains were monitored during and after prestressing, followed by four-point bending tests. The system effectively transferred the prestressing force with minimal losses and no slippage. Beam 1 exhibited a 13.7% immediate strain loss after the second bar was prestressed. Beam 2 was prestressed two times, with average losses of 6.4% and 15.6% on each side after the first bar was prestressed, and 5.0% and 8.0% after the second. After these immediate losses, the prestressing force remained stable. The anchorages performed effectively under bending, maintaining GFRP bars prestress even after concrete crushing.

Keywords

anchors and anchorages, prestressed FRP, GFRP bars, prestressed concrete

Graphical Abstract

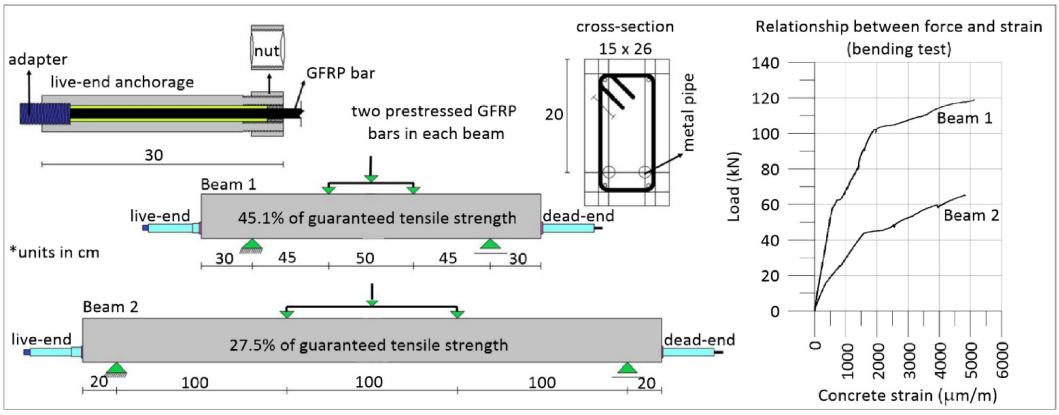

Received February 13, 2026. In revised form February 25, 2026. Accepted March 26, 2026. Available online March 30, 2026.
https://doi.org/10.1590/1679-7825/e9006

1 INTRODUCTION

Corrosion of steel reinforcement is one of the main problems in reinforced concrete structures. Fiber-reinforced polymer (FRP) reinforcement provides an effective alternative due to its corrosion resistance and high strength-to-weight ratio. As FRP materials exhibit high strength only in the longitudinal direction of the fibers (Shi et al., 2015), they are most effectively used as tension-only elements, typically through prestressing techniques (Wang et al., 2015). FRP is a logical choice for prestressed concrete elements to optimize the economic use of these composite materials (Atutis et al., 2015).

Most research on prestressed FRP systems have focused on carbon fiber-reinforced polymer (CFRP), while comparatively limited attention has been paid to glass fiber-reinforced polymer (GFRP) (Zawam et al., 2017). Although CFRP offers higher tensile strength and stiffness, its cost and potential brittleness under certain conditions may limit its use (Jiang et al., 2025). In contrast, GFRP has a lower elastic modulus, which reduces prestress losses, and is also generally more economical than CFRP bars. Additionally, GFRP is chemically resistant, making it ideal for aggressive environments (Jiang et al., 2025). Consequently, GFRP bars represent a balanced solution for prestressed concrete, particularly when cost and durability are prioritized over extreme strength (Jiang et al., 2025). Advances in FRP manufacturing technology have improved the mechanical properties of GFRP bars, enhancing their suitability for prestressed applications (Wang et al., 2022).

When FRP reinforcement is subjected to sustained loading over an extended period, creep strain gradually develops, and this may lead to creep rupture if the load exceeds a critical limit (Rossini and Nanni, 2019). Among FRPs types, CFRP exhibits the most favorable creep performance, followed by basalt FRP (BFRP) and aramid FRP (AFRP), while GFRP is the most susceptible to creep rupture under sustained loading (Zhao et al., 2020). This limits the use of GFRP in prestressing. As the magnitude of the applied load increases, the time to failure decreases (Lignola et al., 2012; Rossini and Nanni, 2019). Consequently, relatively low levels of prestress should be applied to GFRP bars or tendons.

The ACI 440.1R-15 (ACI, 2015) standard provides design guidelines for reinforced concrete structures using FRP reinforcements, including carbon, glass, and aramid fibers. For GFRP, the standard limits sustained stress to 20% of its design tensile strength to prevent creep rupture. This means that the stresses resulting from the unfactored moment, including all sustained loads (dead loads and the sustained portion of live loads), must not exceed this limit (ACI, 2015). The design tensile strength is calculated by multiplying the guaranteed tensile strength by an environmental reduction factor. For GFRP, this factor is 0.7 for concrete exposed to earth and weather, and 0.8 for concrete not exposed (ACI, 2015). Experimental studies on various GFRP bars suggest that the creep rupture reduction factors prescribed by standards are conservative (Esmaeili et al., 2021; Rossini et al., 2019). Additionally, the more recent ACI Code 440.11-22 (ACI, 2022) specifies provisions for structures reinforced exclusively with GFRP bars, including an environmental factor of 0.85 and a sustained stress limit of 30% of the design strength. The fib Model Code for Concrete Structures 2020 (fib, 2024) also addresses creep behavior in FRP materials: The allowable stress level for preventing stress rupture depends on the fiber/resin system, fiber alignment, fiber volume fraction, and environmental exposure. This stress level is specific to the product (fib, 2024). For GFRP, an indicative value for the ratio of creep rupture strength after 100 years to tensile strength is approximately 40% (fib, 2024). Similarly, the fib Model Code 2020 (2024) recommends limiting sustained stresses to prevent creep failure. Environmental exposure of FRP is considered when establishing the creep rupture curve. If this is not done, an environmental reduction factor must be applied, with a typical value of 0.85 (fib, 2024).

Some studies have demonstrated that even limited prestressing values can enhance the structural performance of structural elements with GFRP reinforcement. Atutis et al. (2015) tested beams with prestressed (27% of guaranteed tensile strength) and non-prestressed GFRP bars to investigate aspects related to the serviceability limit state. The prestressed beams had a cracking load 70.6% higher and showed greater stiffness, with more controlled crack growth compared to non-prestressed beams (Atutis et al., 2015). Zawam et al. (2017) tested beams (150 mm x 250 mm x 3600 mm) with prestressed and non-prestressed GFRP bars under monotonic and sustained loading (35%, 60%, or 80% of capacity for 300 days). Three levels of prestressing were considered: non-prestressed, 25% or 40% of the bars' strength (Zawam et al., 2017). Notably, the 40% prestressing level exceeds the limits of sustained loading prescribed by the ACI codes. Prestressing significantly reduced beam deflections under service loading, increased the cracking load, and decreased long-term strains compared to non-prestressed beams (Zawam et al., 2017). Furthermore, the different levels of sustained loading applied over 300 days did not affect the beams' final capacity, indicating minimal impact of creep and relaxation on the GFRP bars' strength (Zawam et al., 2017).

This study investigates the application of prestressing to unbonded GFRP bars. Even when a concrete beam is prestressed with unbonded tendons at a level lower than the balanced ratio for the bonded case, concrete crushing may occur before FRP rupture (Heo et al., 2013; Jeong et al., 2019). The strain in unbonded tendons increases more slowly than in bonded tendons in the critical section, and unbonded tendons can effectively prevent FRP tendon rupture (Lou et al., 2016). Additionally, unbonded tendons have been extensively used due to their fast installation and easy replacement (Lou and Karavasilis, 2018).

Despite offering advantages over traditional steel solutions, a key challenge in the development and widespread adoption of FRP prestressed concrete structures is the anchoring system (Cagnoni et al., 2024). Premature anchor failure is a common failure mode (Wu et al., 2018; Zhao et al., 2020), and conventional steel anchor systems are not recommended for FRP tendons (Al-Mayah et al., 2006; Lignola et al., 2012; Pincheira and Woyak, 2001; Younes et al., 2017; Zhao et al., 2020). The relatively low interlaminar shear strength of the resin matrix requires a longer anchorage length for GFRP composites compared to steel strands (Wolff and Miesseler, 1993).

Given that prestressed GFRP offers advantages despite the limitations of low prestressing levels, and that structures with unbonded prestressed FRP demonstrate greater ductility compared to bonded prestressed FRP, along with the fact that traditional anchorages for steel strands are not suitable for prestressed FRP systems, the objective of this study is to evaluate the effectiveness of a new anchorage system developed for unbonded post-tensioned GFRP bars. The proposed anchorage system incorporates a steel strand in the live-end anchorage, allowing the use of conventional prestressing equipment. In an innovative way, a metal component with the steel strand is threaded into the live-end anchorage and removed after the prestressing force has been applied. An evaluation is conducted on prestressing losses and the performance of the anchorage system in two beams subjected to bending load.

1.1 Research significance

Conventional steel strand anchorages are not suitable for prestressing FRP bars. In some studies, FRP bars have been connected to steel strands using couplers to allow the use of conventional prestressing equipment. This study introduces and evaluates a novel bond-type anchorage system designed for unbonded post-tensioned GFRP bars. Due to limited prestressing levels, few studies exist on GFRP prestressing. The proposed configuration represents a practical advancement: the steel strand is inserted into a metal component, which is then threaded into an adapter located at the live-end anchorage. The metal component can be removed and reused after prestressing. Anchorage tests were performed on full-scale beams, enhancing the practical relevance of the results. The satisfactory performance of the proposed system may encourage further research into GFRP prestressed structural elements. Additionally, the adapter may be incorporated into other anchorage systems for FRP bar prestressing.

2 DESCRIPTION OF THE ANCHORAGE SYSTEM

Live-end and dead-end bond anchorages were developed for post-tensioning unbonded GFRP bars with a commercial diameter of 12 mm. In some studies involving other types of FRP, the FRP bar has been connected to a steel strand using a coupler (Gu and Ansari, 2000; Le et al., 2018, 2019; Liang et al., 2011; Poudel et al., 2022), allowing the use of conventional prestressing equipment designed for steel strands. In these systems, the prestressing force is applied to the steel strand and then transferred to the FRP bar. Similarly, the anchoring system proposed in this study includes a live-end anchorage, where prestressing is applied, and a dead-end anchorage, which serves as the reaction point. A seven-wire steel strand with a nominal diameter of 12.7 mm is used externally at the live-end anchorage, and a nut is used on the live-end anchor to tighten and lock the force after the prestressing has been applied.

A schematic of the developed anchoring system is presented in Figure 1. The live-end and dead-end anchors have the same internal geometries, each consisting of a cylindrical internal structure with a length of 30 cm. This length is similar to the bond-type anchorage system proposed by Gu and Ansari (2000), which was 30.5 cm for 8 mm diameter CFRP bars and 35.6 cm for 10 mm diameter CFRP bars. A nut with an external diameter of 5.5 cm was proposed for the live-end anchorage. The anchors have a 5 cm-long internal thread and a 2 cm-long internal cap, designed to prevent the resin and bar assembly from sliding out of the anchor.

A novel method for inserting the steel strand into the live-end anchorage is proposed in this study. In this approach, the steel strand is inserted into a metal component, which is then threaded into the live-end anchorage. This metal component incorporates a conventional two-piece wedge designed for use in prestressing systems for steel monostrands. The primary advantage of this technique is that the same steel strand can be used to prestress several GFRP bars. After the prestressing force is applied, this metal component can be removed and reused by threading it onto another live-end anchorage, thereby facilitating its repeated use. An adapter, as illustrated in Figures 1 and 2, is internally threaded into the live-end anchor, allowing the subsequent threading of the component containing the steel strand (Figure 3). The adapter is fully threaded along its length.

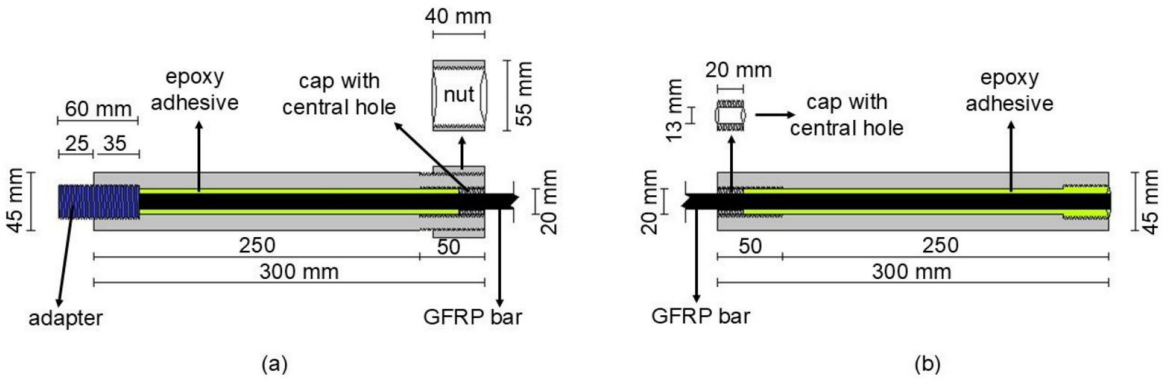

Figure 1 Anchorage system: (a) Live-end anchor; (b) Dead-end anchor.

Figure 2 Adapter.

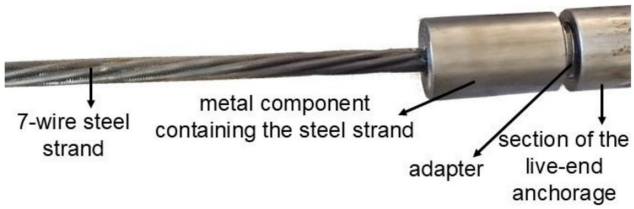

Figure 3 Detail of a section of the live-end anchor: the metal component with the steel strand is threaded into the adapter.

A surface treatment is proposed for the bar to improve its adhesion to the epoxy resin. The treatment was applied to the portion of the bar corresponding to the length in the anchoring area. Initially, isopropyl alcohol was applied to the surface of the bar, followed by a coating of sand with epoxy resin to increase adhesion. To preserve some of the ribs on the bar, the sand treatment was not applied to the entire anchoring length, as shown in Figure 4. The ribs also contribute to adhesion and help prevent the bar from sliding. The bar was placed horizontally on a table, and the sand treatment was applied to three 3 cm-long sections on the live end. The bar was then rotated 180°, and the sand treatment was applied to the opposite side in a further two 3 cm-long sections. After 24 hours, any loose particles that might affect adhesion were removed using water. Following a further 24-hour period, the bar was inserted into the anchorage. Sand treatment on the dead end was carried out with the bar already in position on the beam, the live-end anchor filled with epoxy resin, and the cap pre-installed on the bar. Table 1 summarizes the key dimensions associated with the proposed anchoring system.

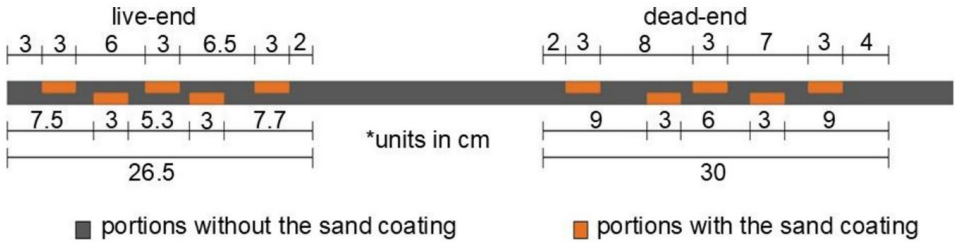

Figure 4 Schematic of the sand coating along the anchorage lengths.

This study also proposes a method for assembling and preparing the bar system and anchorages. A metal plate with a central hole is fixed to the concrete surface to protect it during prestressing, ensuring the anchorages do not contact the concrete directly. The anchors are first cleaned using paper, cloth, degreaser and isopropyl alcohol. The live-end anchor, already containing the adapter, was positioned vertically. Epoxy adhesive was applied to the live-end anchor outside the structure, and the bar was then inserted. After curing, the bar-anchorage assembly is inserted into the structure, and the dead-end anchorage is installed. A wooden disc with a pre-drilled hole is attached to the dead-end anchor, and epoxy is injected using a syringe and a thin hose. Duct tape is used together with the wooden disc to ensure that only three openings remain at the anchorage end: for the bar, the hose, and air escape. The hose was gradually removed as the adhesive was injected. To simplify the process, a short length of bar was left extending from the dead-end anchorage. Prestressing is applied no earlier than seven days after injection, based on the resin properties. A two-component, low-viscosity epoxy gel resin was used to fill the anchorages and coat sections of the sanded GFRP bars. Classified as a structural adhesive, the resin was chosen for its high fluidity, which allowed easy and complete filling of the anchorages, minimizing voids. Initially, components A and B were individually homogenized. They were then manually mixed in a 2:1 ratio for 5 minutes at a slow pace, resulting in a homogeneous mixture. Curing was performed at room temperature. Even in the dead-end anchorages, which were filled with resin while in the horizontal position, a syringe and hose were used to facilitate the filling process.

Table 1 Summary of dimensions related to the proposed anchoring system.

	Live-end anchor	**Dead-end anchor**
Total tube length	30 cm	30 cm
Internal threaded length	5 cm	5 cm
Cap length with internal hole	2 cm	2 cm
Length with internal thread for adapter	3.5 cm	3.5 cm
Adapter length	6 cm (with 3.5 cm internally threaded into the anchorage)	- *
GFRP bar length inside the anchorage	26.5 cm	30 cm
Sand coating length	Three 3 cm sections and two 3 cm sections	Three 3 cm sections and two 3 cm sections

*The adapter is only inserted into the live-end anchorage.

3 MATERIALS AND METHODS

Two beams were fabricated to evaluate the anchorage system under realistic conditions. In the first beam, each bar was prestressed to 45.1% of its guaranteed tensile strength. Concrete strains were measured during prestressing to evaluate immediate losses and were subsequently monitored over 134 hours, including a 20-hour interruption. Each bar in the second beam was prestressed to 27.5% of its guaranteed tensile strength, and strains were monitored during prestressing and for 48 hours thereafter. Both beams were later tested under four-point bending to evaluate the anchorage performance under load.

3.1 GFRP bars

GFRP bars with a nominal diameter of 12 mm were used to test the anchorages. According to the manufacturer, these bars are produced via the pultrusion process, using fibers and epoxy resins (a polymer matrix with hardener and pigment). Tests were conducted to determine the effective diameter using the underwater weighing method, in accordance with ABNT NBR17201-2 (ABNT, 2025). Tensile tests were performed following the procedures specified in ASTM D7205/D7205M-21 (ASTM, 2021). Five specimens were used in each test, representing the batch of GFRP bars. Due to the limited maximum stroke length of the testing machine, specimens with a total length of 80 cm were used in the tensile tests. Each specimen consisted of 30 cm of free length and 25 cm designated for the anchors. The effective diameter of the bars was found to be 11.60 mm, with a standard deviation of 0.12 mm. The average tensile strength was 891.9 MPa, with a standard deviation of 23.0 MPa. The average modulus of elasticity was 50,351 MPa, and the estimated ultimate tensile strain reached 0.0177. The guaranteed tensile strength is defined as the average tensile strength minus three times the standard deviation (ACI, 2015), resulting in a value of 822.9 MPa.

3.2 Beam 1 – Evaluation of prestressing losses

Beam 1 is 2 meters in length, with a cross-section of 15 cm × 26 cm (width × height). A ready-mixed concrete with a characteristic compressive strength of 30 MPa at 28 days was used. Compressive strength tests were conducted at 90 days

on five cylindrical specimens (100 mm x 200 mm), in accordance with ABNT NBR 5739 (2018). The average compressive strength was 46.70 MPa, with a standard deviation of 5.01 MPa. Modulus of elasticity tests were also performed at 90 days on three specimens of the same dimensions, following ABNT NBR 8522-1 (2021). The average modulus of elasticity was 38.17 GPa, with a standard deviation of 0.41 GPa.

The beam was prestressed with two unbonded GFRP bars, positioned 20 cm from the top fiber of the concrete to the centroid of the prestressing bars. It was reinforced with three steel stirrups and four longitudinal steel bars, all 6.3 mm in diameter. The longitudinal bars provided constructive reinforcement, while the stirrups were placed outside the shear span. Prior to concrete casting, two metal pipes (21 mm outer diameter, 0.6 mm thickness) were installed as ducts at the level of the GFRP bars. The arrangement of the steel pipes and reinforcement is shown in Figure 5. After concrete curing, one GFRP bar was inserted into each pipe. A metal plate with two holes was bonded externally to each side of the beam to prevent damage to the concrete during the locking of the prestressing force. Prestressing was applied individually to each bar.

The beam was simply supported over a 1.4 m span during the application and monitoring of the prestressing force. Prestressing was applied to the GFRP bars 256 days after casting. Each bar was subjected to a prestressing force of approximately 39.2 kN, corresponding to 45.1% of its guaranteed tensile strength. A prestress level higher than that recommended by current standards for sustained loading of GFRP bars was intentionally adopted to validate the anchorage system for future use with GFRP bars of higher creep rupture strength. This prestressing level is used only to validate the proposed anchoring system and is not a practical design recommendation for typical GFRP bars.

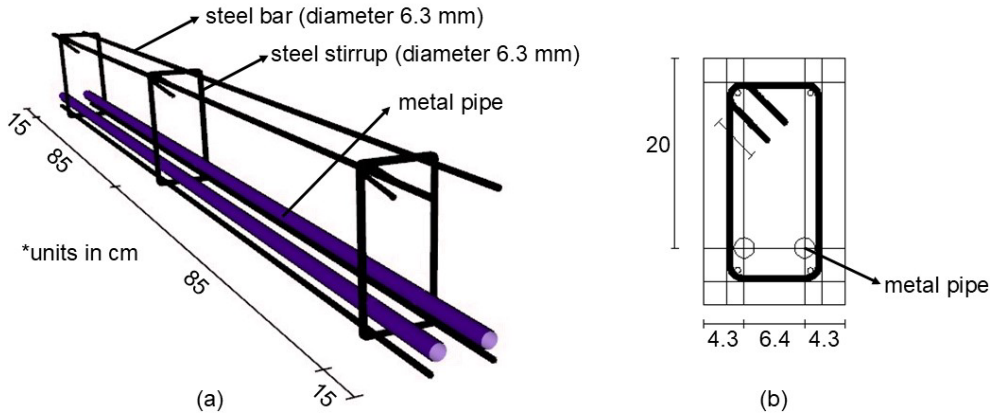

Figure 5 Reinforcement and steel pipe configuration of Beam 1: (a) Schematic illustration of the steel bars and pipes; (b) Positioning of the pipes within the cross-section.

Strain gauges were installed on the concrete to monitor strains. A quarter-bridge strain gauge was positioned on one side of the beam at the level of the GFRP bar, recording at a rate of one reading per second during and immediately after prestressing. On the opposite side, a temperature-compensated half-bridge strain gauge was installed at the same height, recording data at a rate of one reading per hour, along with a vertical strain gauge to compensate for temperature effects (Figure 6). The strain gauges on both sides were installed at a distance of 20 cm from the support closest to the live end. Strains were monitored for 134 hours after prestressing, with a 20-hour interruption. Two HBM Spider 8 data acquisition systems were employed: one for recording strain during prestressing at one reading per second, and the other for post-prestressing at one reading per hour. Each system was connected to a separate computer running CATMAN 4.5 software. A photograph of the monitoring setup is shown in Figure 7.

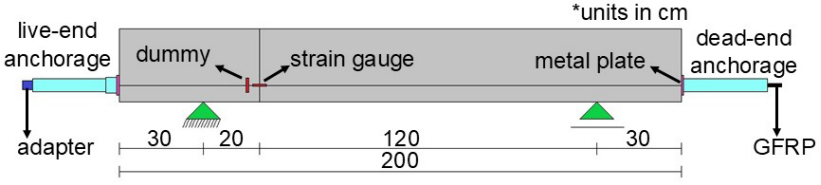

Figure 6 Beam 1: Schematic of the temperature-compensated half-bridge strain gauge.

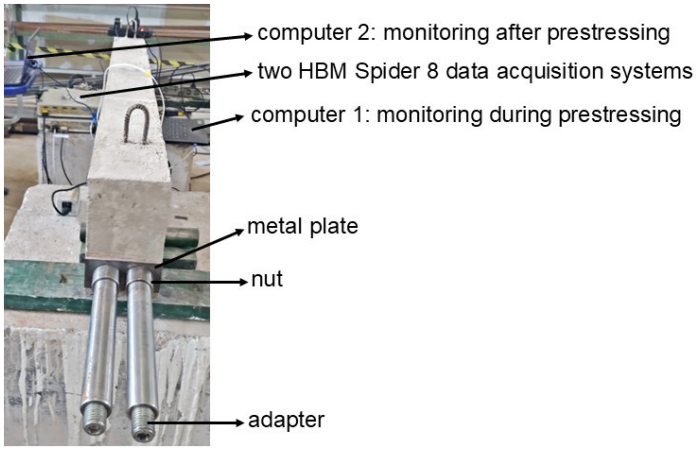

Figure 7 Beam 1 during the strain monitoring phase (view of the live-end anchorage).

3.3 Beam 2 – Evaluation of prestressing losses

Beam 2 had an overall length of 3.4 meters and a rectangular cross-section measuring 15 cm × 26 cm (width × height). Ready-mixed concrete with a characteristic compressive strength of 30 MPa at 28 days was used. Compressive strength and modulus of elasticity tests were performed at 28 days on cylindrical specimens (100 mm × 200 mm), following ABNT NBR 5739 (2018) and ABNT NBR 8522-1 (2021). Nine specimens were tested for compressive strength and three for modulus of elasticity. The average compressive strength was 45.93 MPa (standard deviation of 7.38 MPa), and the average modulus of elasticity was 32.11 GPa (standard deviation of 3.95 GPa).

Beam 2 has the same cross-section, steel bars, and pipes as Beam 1 (Figure 5(b)). Concrete casting, GFRP bar insertion, and prestressing procedures were also identical. However, Beam 2 contains 25 stirrups (6.3 mm diameter) spaced at 12.5 cm intervals along its length. Reinforcement details are shown in Figure 8. The beam, simply supported over a 3.0 m span, was prestressed 154 days after casting. Each GFRP bar was prestressed to approximately 24.0 kN, corresponding to 27.5% of its guaranteed tensile strength, similar to the value used by Atutis et al. (2015). In this second beam, the live-end anchor nut and external thread lengths were increased to 60 mm and 70 mm, respectively, to allow greater bar elongation (a modification recommended for future studies).

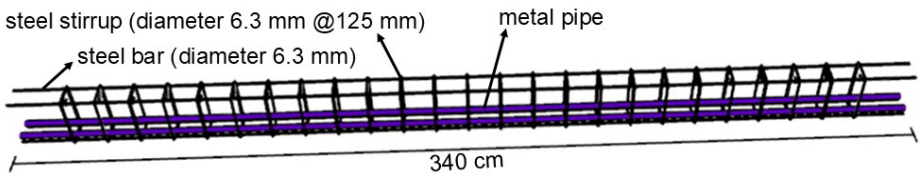

Figure 8 Reinforcement and steel pipe configuration of Beam 2.

Two strain gauges were installed on Beam 2, one on each side, 20 cm from the support near the live anchorage at the level of the GFRP bars. A temperature-compensated half-bridge gauge was placed on one side, and a quarter-bridge gauge on the opposite side. For the half-bridge strain gauge, the temperature compensation gauge was bonded to a separate concrete element (Figure 9). During prestressing, strains were recorded on both sides at one reading per second. For comparison, a prestressing force was applied to both GFRP bars and then released. The bars were prestressed a second time, providing two strain measurements per side. After the second prestressing, measurements were stopped. A new monitoring was conducted for 48 hours at a rate of one reading per hour using the temperature-compensated half-bridge gauge.

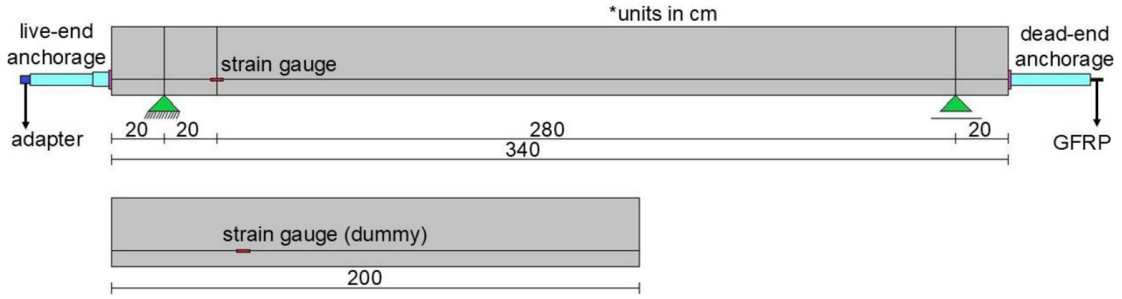

Figure 9 Beam 2 – Schematic of the temperature-compensated half-bridge strain gauge.

3.4 Bending tests

When designing an anchorage system, it is essential to ensure its effectiveness up to the ultimate limit state and to prevent failure at the anchorage zones. To evaluate the performance of the anchorages in structural elements under bending loads, the beams were tested to failure under four-point bending. The two experimental setups are illustrated in Figure 10. Beam 1 was tested when the concrete was 353 days old, with prestressing applied 97 days earlier. Beam 2 was tested when the concrete was 166 days old, with prestressing applied 12 days earlier. In both cases, the load was applied at mid-span using a hydraulic jack, and transferred to the concrete beam through a steel distribution beam supported by two I-beams. A strain gauge was bonded to the top surface at mid-span to measure concrete strain. Beam 1 was instrumented with two Linear Variable Differential Transformers (LVDTs) positioned at mid-span to measure vertical deflections, one on each side, while Beam 2 had both LVDTs on the same side. The applied load was monitored using a 500 kN load cell. Loading rates were approximately 0.03 kN/s for Beam 1 and 0.06 kN/s for Beam 2, with data acquired at one reading per second.

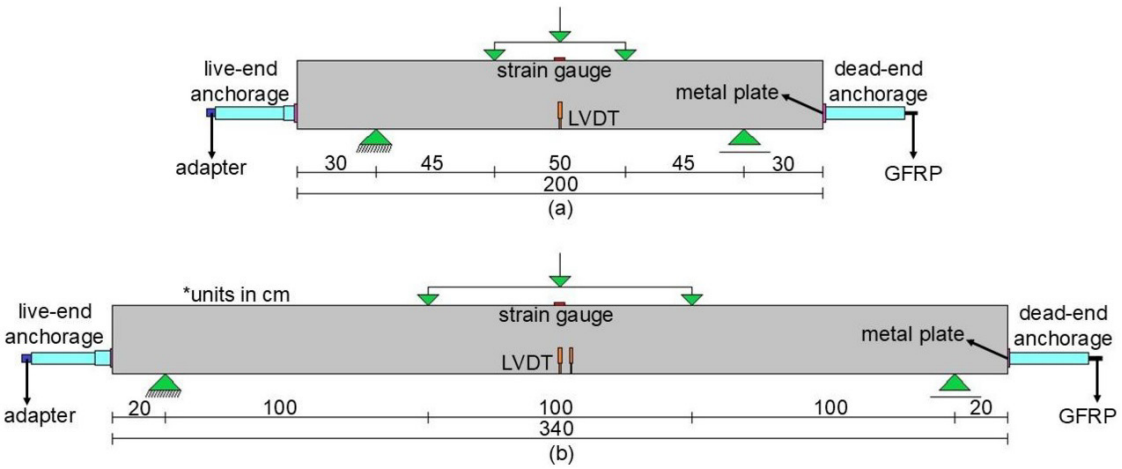

Figure 10 Schematic of the bending test configuration: (a) Beam 1; (b) Beam 2.

4 RESULTS AND DISCUSSIONS

4.1 Evaluation of prestressing losses

The proposed anchorage system, in combination with epoxy resin, proved effective in transferring the prestressing force to GFRP bars. Prestressing was successfully applied to Beams 1 and 2, reaching target loads of 39.2 kN and 24.0 kN, respectively. The strain behavior during prestressing is shown in Figure 11. For Beam 1 (Figure 11(a)), an immediate loss in prestressing strain of approximately 13.7% was recorded following the application of the prestressing force to the second GFRP bar. To calculate this value, the average strain immediately after prestressing (117.0 μm/m) and the average strain after the losses (101.0 μm/m) were determined, and the percentage loss was obtained from the relative difference between these two averages. However, it was not possible to quantify the individual contributions of different mechanisms – such as anchor accommodation, bar slippage, friction, or elastic shortening of the concrete – to this initial loss. Despite some noise in the measured data, the graph shows a constant trend after the immediate losses, indicating that the prestress force remained stable over time. Due to fluctuations in the recorded data, it was not possible to precisely quantify the percentage loss after the prestressing of the first GFRP bar.

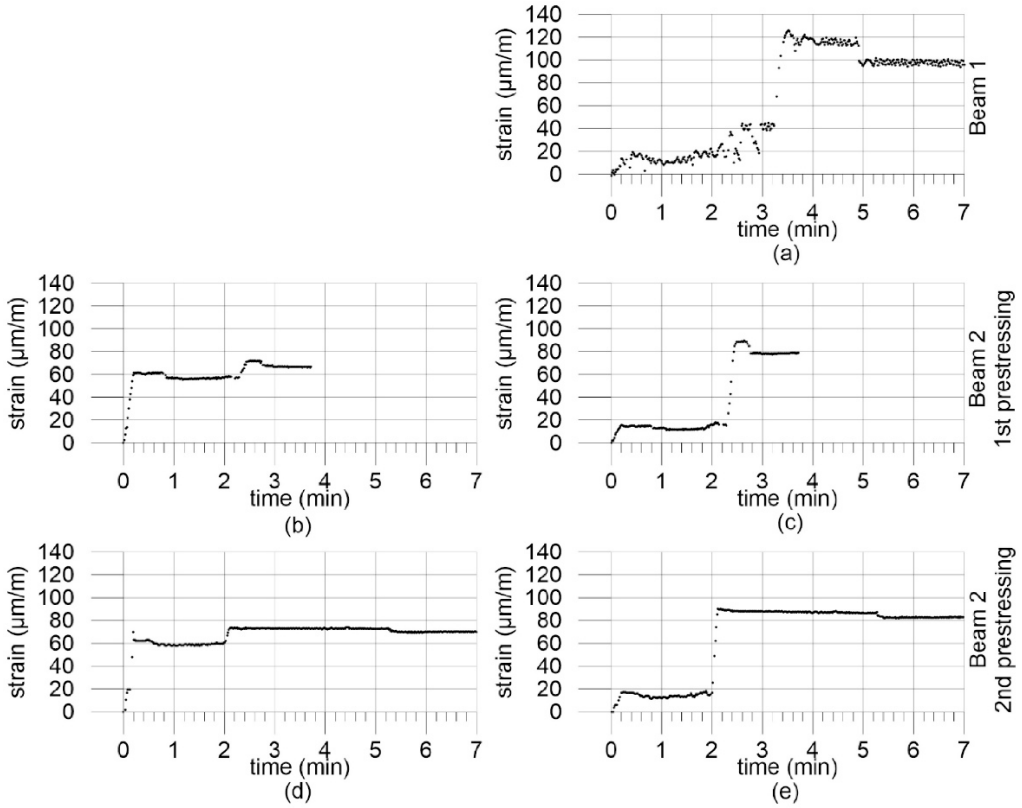

Figure 11 Concrete strains during prestressing: (a) Beam 1 – side face closest to the second prestressed bar; (b) Beam 2 – first prestressing, side face closest to the first prestressed bar; (c) Beam 2 – first prestressing, side face closest to the second prestressed bar; (d) Beam 2 – second prestressing, side face closest to the first prestressed bar; (e) Beam 2 – second prestressing, side face closest to the second prestressed bar.

Figures 11(b) and 11(c) show the concrete strain measurements during the first prestressing of Beam 2 on the side faces closest to the first and second prestressed GFRP bars, respectively. Figures 11(d) and 11(e) present the corresponding results from the second prestressing stage on the same faces. The strain behavior on the face near the first prestressed bar (Figures 11(b) and 11(d)) was similar, with average strains of 61.1 μm/m and 62.4 μm/m (2.1% higher) after the first bar was prestressed, and 71.8 μm/m and 72.8 μm/m (1.4% higher) after the second bar was prestressed. Similarly, for the face closest to the second prestressed bar (Figures 11(c) and 11(e)), the strain values were also similar. The average strains were 14.8 μm/m and 16.5 μm/m (11.5% higher) after the first bar was prestressed, and 88.1 μm/m and 87.1 μm/m (1.1% lower) after the second bar was prestressed. In the two prestressing stages of Beam 2, the face closest to the second prestressed bar exhibited greater strain after the second bar was tensioned, with an average increase of 21.1% compared to the opposite side. Overall, the strain results from both tests on Beam 2 demonstrated a high degree of similarity, indicating consistency in the experimental data.

Table 2 presents the concrete strain losses observed in the two tests on Beam 2, expressed in both absolute and percentage terms, based on data from Figures 11(b)–(e). The results consider average strain values. The percentage of prestress losses was calculated in the same manner as described previously for Beam 1: the average strain before the losses and the average strain after the losses were determined, and the percentage reduction between these two values was then calculated. Overall, percentage losses were similar for the same face after prestressing either the first or second bar. The only exception was the face closest to the second bar after its prestressing, where losses differed between the two tests (9.7 μm/m during the first prestressing of the beam and 4.2 μm/m during the second). During the prestressing of the first bar, the face furthest from it showed greater percentage losses but smaller absolute losses. This is because the strains on the face closest to the first prestressed bar were, on average, four times higher than those on the opposite face. In general, immediate concrete strain losses were low. After prestressing the first bar, the average percentage losses were 6.4% and 15.6% on the faces closest and furthest from this bar, respectively. After prestressing the second bar, these values were 5.0% and 8.0%. These results indicate that the proposed anchorage performs effectively during prestressing. A direct comparison of strain losses between Beams 1 and 2 is not feasible due to differences in their dimensions, reinforcement configurations, concrete composition, and prestressing ages.

Table 2 Concrete strain losses in Beam 2: absolute and percentage values.

	Test 1: First prestressing of the beam		Test 2: Second prestressing of the beam	
	Side face 1 [(a)]	Side face 2 [(b)]	Side face 1 [(a)]	Side face 2 [(b)]
Average strain before the first prestress loss	61.1 μm/m	14.8 μm/m	62.4 μm/m	16.5 μm/m
Average strain after the first prestress loss	56.7 μm/m	12.7 μm/m	58.9 μm/m	13.8 μm/m
Average strain before the second prestress loss	71.8 μm/m	88.0 μm/m	72.8 μm/m	87.1 μm/m
Average strain after the second prestress loss	67.5 μm/m	78.3 μm/m	69.9 μm/m	82.8 μm/m
Losses after prestressing of the first GFRP bar	4.4 μm/m 7.3%	2.1 μm/m 14.5%	3.4 μm/m 5.5%	2.8 μm/m 16.7%
Losses after prestressing of the second GFRP bar	4.3 μm/m 6.1%	9.7 μm/m 11.1%	2.9 μm/m 4.0%	4.2 μm/m 4.9%

[(a)] Lateral face 1 of the beam corresponds to the side closest to the first prestressed GFRP bar. [(b)] Lateral face 2 of the beam corresponds to the side closest to the second prestressed GFRP bar.

A simplified calculation of concrete stresses due to the prestressing force was carried out, as detailed in Appendix A, without considering prestressing losses. Stresses were determined at four points defining the cross-section and at two locations corresponding to the height of the prestressing force, where the strain gauges were attached, as described in Sections 3.2 and 3.3. The prestressing force was applied one bar at a time, with the beams simply supported during testing. Only strains induced by prestressing were recorded. Therefore, no stress calculations related to dead weight were performed. Eccentricities in both directions were considered, as the prestressing force was not applied at the section centroid. For Beam 1, the calculated stresses after prestressing the first GFRP bar – excluding losses – were 3.17 MPa (compression) on the nearest face and 0.59 MPa (compression) on the opposite face at the height of the bars. After prestressing of the second bar, the combined effect of both resulted in calculated compressive stresses of 3.76 MPa. Figure 11(a) shows the response of the strain gauge positioned closest to the second prestressed bar. At this location, the ratio of recorded strains after prestressing the second bar to those after prestressing the first bar was approximately 117 μm/m to 20 μm/m, corresponding to a ratio of about 5.85. The ratio of the calculated stresses at the same location was 3.76 MPa to 0.59 MPa, corresponding to 6.37. These results show close agreement, and the measured strain distribution in the beam is consistent with the stress distribution predicted by the theoretical model.

For Beam 2, the calculated concrete compressive stresses at the bar level after prestressing the first GFRP bar were 1.94 MPa and 0.36 MPa on the faces closest and furthest from the bar, respectively (see Appendix A). After both bars were prestressed, the final calculated stress on each face was 2.30 MPa. On the face nearest the first GFRP bar (Figures 11(b) and 11(d)), the calculated stress ratio (2.30 MPa to 1.94 MPa) was 1.19, while the measured strain ratios (excluding prestress losses) were 1.18 and 1.17. On the opposite face, the calculated stress ratio was 6.39, while the corresponding measured strain ratios in Figures 11(c) and 11(e) were 5.94 and 5.26, respectively. Overall, the measured strains in Beam 2 also show good agreement with the stress distribution predicted by the theoretical model. Further studies are recommended to evaluate the influence of prestressing losses in stress calculations for GFRP prestressed beam using the proposed anchorage system.

Based on the stresses calculated in Appendix A, the corresponding concrete strains were estimated for comparison with the experimental results, as shown in Table 3. The experimental values represent the average of the data used to generate the graphs in Figure 11. These values correspond to the mean strain measured after prestressing the first or second bar, before the occurrence of prestress losses. Strains were estimated by dividing the calculated stresses (Appendix A) by the experimentally determined initial modulus of elasticity reported in Sections 3.2 and 3.3. The concrete modulus of elasticity was determined at 90 days for Beam 1 and at 28 days for Beam 2, while prestressing was applied at 256 and 154 days, respectively. Despite the differences between the ages at which the modulus of elasticity was tested and prestressing was applied, the experimentally determined modulus was adopted for the strain calculations in a simplified approach. For each beam, the first calculated strain neglected prestress losses. A second strain calculation was performed to account for the influence of prestress losses after prestressing the first bar on the strain after prestressing the second bar. This was done by subtracting the absolute value of the losses after prestressing the first bar (Table 2) from the strain calculated for the second bar.

The absolute differences between calculated and experimental strains after prestressing the first GFRP bar were minimal in all three tests, with a maximum difference of 5.2 μm/m observed on side 2 of the second test of Beam 2. For the strains measured after prestressing the second bar, the experimental values were closer to the calculated values that did not account for prestress losses from the first bar. These higher experimental values may be attributed to the greater influence of concrete's nonlinear behavior during the prestressing of the second bar, which was not considered in the calculations.

At low stress levels, concrete behaves nearly linearly, but nonlinear effects become more significant as stress increases. Despite this, the experimental and calculated remain in reasonably good agreement. Even without considering the concrete's initial elastic modulus at the age of prestressing, the estimated strains closely match the experimental values, indicating that the beam's behavior aligns well with the predictions. The largest absolute differences between experimental and calculated strains (without considering prestress losses) after prestressing the second bar occurred on side 2 (the side closest to the second prestressed GFRP bar), with values of 18.5 μm/m for Beam 1 and 16.3 μm/m and 15.3 μm/m for Beam 2 in tests 1 and 2, respectively. In percentage terms, these values correspond to differences of 15.8%, 18.5%, and 17.6%, respectively. In contrast, differences on side 1 (the side closest to the first prestressed GFRP bar) were minimal, measuring only 0.1 μm/m and 1.1 μm/m for Beam 2 in tests 1 and 2.

Table 3 Estimation of concrete strains and comparison with experimental results.

Beam 1 [c]				
	Side face 1 [a]		**Side face 2 [b]**	
	After prestressing of the first GFRP bar	After prestressing of the second GFRP bar	After prestressing of the first GFRP bar	After prestressing of the second GFRP bar
Experimental strain			17.1 μm/m	117.0 μm/m
Calculated strain [d]			15.5 μm/m	98.5 μm/m
Calculated strain minus losses after prestressing of the first bar [e]				[f]
Beam 2: Test 1 – First prestressing of the beam [c]				
	Side face 1 [a]		**Side face 2 [b]**	
	After prestressing of the first GFRP bar	After prestressing of the second GFRP bar	After prestressing of the first GFRP bar	After prestressing of the second GFRP bar
Experimental strain	61.1 μm/m	71.8 μm/m	14.8 μm/m	88.0 μm/m
Calculated strain [d]	60.4 μm/m	71.7 μm/m	11.3 μm/m	71.7 μm/m
Calculated strain minus losses after prestressing of the first bar [e]		67.3 μm/m		69.6 μm/m
Beam 2: Test 2 – Second prestressing of the beam [c]				
	Side face 1 [a]		**Side face 2 [b]**	
	After prestressing of the first GFRP bar	After prestressing of the second GFRP bar	After prestressing of the first GFRP bar	After prestressing of the second GFRP bar
Experimental strain	62.3 μm/m	72.8 μm/m	16.5 μm/m	87.0 μm/m
Calculated strain [d]	60.4 μm/m	71.7 μm/m	11.3 μm/m	71.7 μm/m
Calculated strain minus losses after prestressing of the first bar [e]		68.4 μm/m		68.9 μm/m

[a] Lateral face 1 of the beam corresponds to the side closest to the first prestressed GFRP bar. [b] Lateral face 2 of the beam corresponds to the side closest to the second prestressed GFRP bar. [c] The experimental values of the initial elastic modulus were adopted in the strain calculations. For Beam 1, the average initial elastic modulus at 90 days was 38.17 GPa. For Beam 2, the average initial elastic modulus at 28 days was 32.11 GPa. [d] The first strain calculation was performed assuming that no prestress losses occur. [e] A second calculation was performed assuming that the experimental prestress losses after prestressing the first bar (Table 2) may affect the strain immediately after prestressing the second bar. [f] Due to fluctuations in the recorded data, it was not possible to precisely quantify the prestress loss after the prestressing of the first GFRP bar of Beam 1.

The strain monitoring results after prestressing are shown in Figure 12. Some noise was observed, possibly due to daily temperature fluctuations, even though a temperature-compensated half-bridge gauge was used. This did not compromise the overall conclusions. For Beam 1, the strain values recorded during the monitoring phase (Figure 12(a)) were higher than those observed during prestressing (Figure 11(a)). The post-prestressing gauge was located on the face closest to the first GFRP bar, where lower strain levels were observed in Beam 2. Measurements in Beam 1 were collected using different data acquisition systems, which may have contributed to this discrepancy. Despite noise and this discrepancy, the strain data exhibited a constant trend throughout the monitoring period, indicating that the proposed anchorage length and surface preparation effectively maintained the prestressing force.

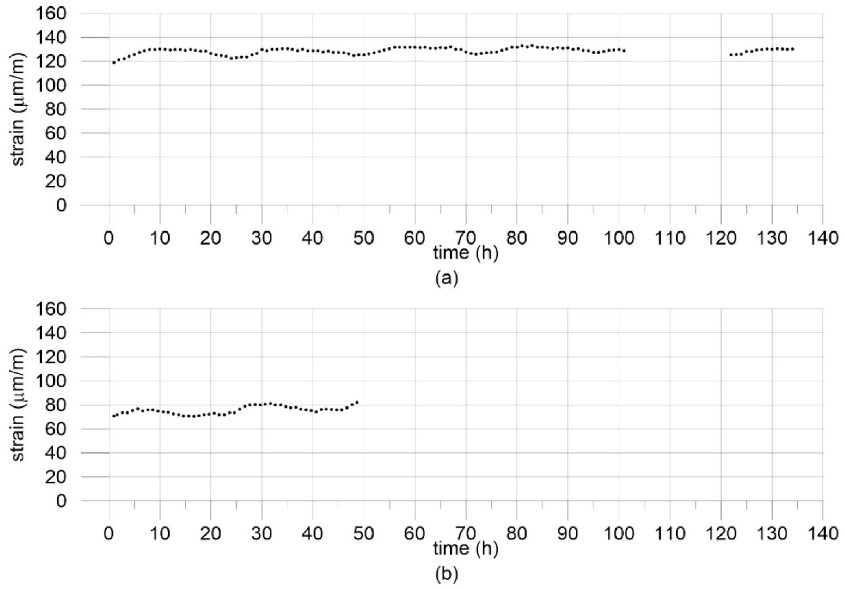

Figure 12 Concrete strains after prestressing on the face closest to the first prestressed GFRP bar: (a) Beam 1; (b) Beam 2.

4.2 Bending tests

During the bending tests on Beams 1 and 2, no slippage of the GFRP bars from the anchorages was observed. The anchorage system performed effectively throughout loading, with no issues detected up to the ultimate load. Both beams failed due to concrete crushing in the compression zone, indicating a flexural failure mode, as shown in Figure 13. As the bending load was removed, the prestressing force caused the beams to recover their original shape, with minimal deflection and partial crack closure. Therefore, the GFRP bars remained prestressed even after concrete crushing. The anchorages also continued to function properly after failure and showed no visible damage at any stage. Similar behavior was reported by Zawam et al. (2017), who observed partial crack closure in the tension zone after removal of loading in beams with prestressed GFRP reinforcement. Residual partial crack closure was evaluated only qualitatively in this study; future research is recommended to quantitatively assess the residual deflection after unloading.

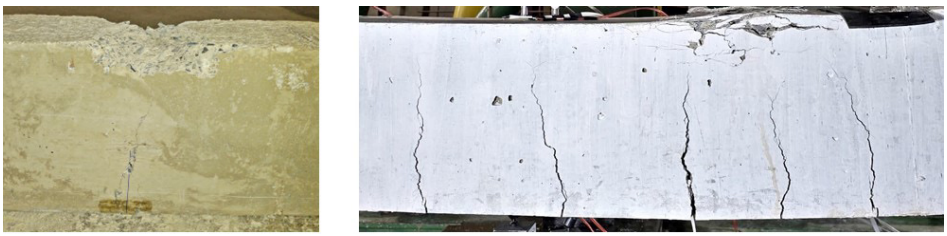

Figure 13 Failure modes: (a) View of the central region of Beam 1 after flexural failure (concrete crushing) and unloading; (b) Beam 2 – concrete crushing after the bending test.

The relationship between force and midspan deflection is shown in Figure 14, while the relationship between force and concrete strain is shown in Figure 15. Both graphs show similar trends for each beam. A linear response was observed up to about 60 kN in Beam 1 and 16 kN in Beam 2, corresponding to the uncracked state. These load levels correspond to the cracking loads of the respective beams. Beam 1 exhibited greater stiffness, as indicated by the steeper slope in the elastic region of the two graphs. The maximum load and deflection were 125.5 kN and 44 mm for Beam 1, and 65.3 kN and 109 mm for Beam 2. The larger deflection observed in Beam 2 was attributed to its longer bending span and lower prestressing force. Since the failure occurred due to concrete crushing, a portion of the concrete in the central region of the beam detached near the end of the test. The maximum concrete strain at the center of the beam's top surface was 5122 µm/m for Beam 1 and 4821 µm/m for Beam 2.

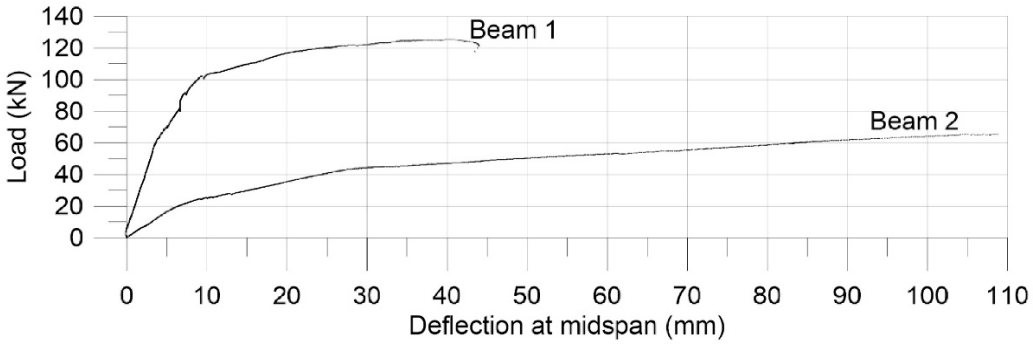

Figure 14 Relationship between force and deflection at midspan.

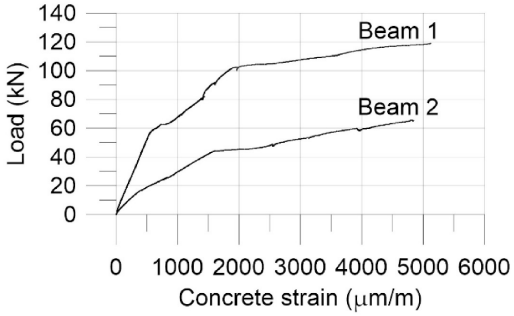

Figure 15 Relationship between force and concrete strain.

One of the main concerns in the design of FRP-reinforced or FRP-prestressed structures is the evaluation of service-load deflection, as these deflections are generally larger than those in steel-reinforced or steel-prestressed structures. To evaluate the service-load deflection, the procedure proposed by Alraie and Matsagar (2023) was followed. In their study, four series of beams reinforced with BFRP bars, either prestressed or non-prestressed, were tested. The service load was determined from the experimental ultimate flexural load by applying a strength reduction factor of 0.7 and then dividing by a load factor of 1.7. Once the service load was defined, the corresponding deflection was obtained from the load–deflection curve and taken as the service-load deflection. Using this approach, the service loads for Beams 1 and 2 were 51.7 kN and 26.9 kN, respectively, with corresponding midspan deflections of 3.0 mm and 11.8 mm. Alraie and Matsagar (2023) also compared these experimental values with the permissible deflection of L/240, as specified in ACI 440.1R-15. Considering L as the span length between supports, the permissible deflections are 5.83 mm for Beam 1 and 12.5 mm for Beam 2. Therefore, both beams satisfy the serviceability deflection criterion.

4.3 Limitations of the study

This study has some limitations that should be considered. The limited number of specimens tested (two prestressed beams with different levels of prestressing) may restrict the general applicability of the results and may not fully represent the variability in material behavior. However, the use of full-scale beams enhances the practical significance of the results. Despite these limitations, the study provides valuable insight into the performance of the proposed anchorage system for unbonded post-tensioned GFRP bars. In one beam, the applied prestressing exceeded the sustained load limit recommended in current standards, yet the anchors performed effectively. Further research with more specimens is recommended to confirm these findings and to better assess prestressing losses associated to the proposed anchorage system. Another limitation is that only 12 mm diameter GFRP bars were tested. Additional studies should evaluate the performance of the anchorage system with GFRP bars of different diameters, considering the necessary adjustments in anchorage lengths. The anchorage performance is mainly governed by the anchorage length, resin properties, bar surface treatment, bar diameter, and the applied stress level. The presence of the cap and the internal threads should also be considered in future studies, as they contribute to the mechanical performance of the proposed anchorage system.

5 CONCLUSIONS

A specific anchorage system was developed to apply prestressing to unbonded GFRP bars with a commercial diameter of 12 mm. The system comprises two components: a live-end anchorage, where the prestressing force is applied, and a dead-end anchorage, which provides passive reaction. A steel strand is connected to the live-end anchorage, which contains the GFRP bar. The prestressing force is applied to the steel strand and subsequently transferred to the GFRP bar.

In a novel approach, the steel strand is inserted into a metal component that is threaded into a metal adapter connected to the live-end anchorage containing the GFRP bar. After prestressing, the component with the steel strand can be removed and reused by threading it onto another live-end anchorage, enabling prestress to be applied to additional GFRP bars. This threaded connection method is simpler and more practical than directly coupling the FRP bar and steel strand inside mechanical couplers, as has been done in some studies. The proposed adapter, or similar alternatives, could be integrated into various existing FRP anchorage systems to simplify the prestressing process.

Larger anchorages are required for FRP bars compared to those typically used for steel strands. The selected anchorage length proved adequate, as no prestress losses due to bar slippage were observed – an issue commonly associated with insufficient anchorage. In the first beam tested with the proposed anchoring system, an immediate prestress loss of approximately 13.7% was recorded after prestressing the second GFRP bar. A second beam was prestressed two times, showing similar strain behavior. After prestressing the first bar, the average losses were 6.4% and 15.6% on the faces closest to and furthest from the bar, respectively. After prestressing the second bar, these values were 5.0% and 8.0%. The prestressing force remained stable in the short-term after transfer under laboratory conditions. Beam 1 was monitored for 134 hours, including a 20-hour interruption, while Beam 2 was monitored for 48 hours. No significant progressive prestress losses were observed. The anchorage length and surface treatment were effective in maintaining the applied prestressing force with minimal loss. Overall, the proposed system was effective in both applying and sustaining the prestressing force throughout the monitoring period.

The anchorages also performed well during the bending tests, with no GFRP bar slippage observed. After failure and unloading, the prestressing force enabled the beam to return to its original shape, with minimal deflection and partial crack closure. This indicates that the GFRP bars remained prestressed even after concrete crushing. The anchorage system continued to perform effectively even after the beam failure.

Acknowledgements

The authors gratefully acknowledge Lorenzini Protensão (Grupo Impacto: Brasília-DF) for all their support during the production and testing of the anchorages. This study was financed in part by the Coordenação de Aperfeiçoamento de Pessoal de Nível Superior – Brasil (CAPES) – Finance Code 001. The authors would like to acknowledge the Conselho Nacional de Desenvolvimento Científico e Tecnológico (CNPq) - process number 423662/2018-0. We gratefully acknowledge the financial support provided by DPI/BCE/UnB under the Call Notice DPI/BCE/UnB No. 001/2026.

Author's Contribuitions: Conceptualization, LF Borges and RdeM Lameiras; Formal Analysis, LF Borges; Methodology, LF Borges and RdeM Lameiras; Investigation, LF Borges and RdeM Lameiras; Project Administration, RdeM Lameiras; Writing - original draft, LF Borges; Writing - review & editing, LF Borges and RdeM Lameiras; Funding acquisition, LF Borges and RdeM Lameiras; Supervision, RdeM Lameiras

Data Availability: Research data is available in the body of the article

Editor: Marcílio Alves

References

ABNT NBR 8522-1 (2021). Concreto Endurecido - Determinação Dos Módulos de Elasticidade e de Deformação. Parte 1: Módulos Estáticos à Compressão. Associação Brasileira de Normas Técnicas, Brasil.

ABNT NBR17201-2 (2025). Barras de Polímero Reforçado Com Fibras (FRP) Destinadas a Armaduras Para Estruturas de Concreto Armado. Parte 2: Determinação Do Diâmetro Efetivo. Associação Brasileira de Normas Técnicas, Brasil.

ABNT NBR5739 (2018). Concreto - Ensaio de Compressão de Corpos de Prova Cilíndricos. Associação Brasileira de Normas Técnicas, Brasil.

ACI 440.11-22 (2022). Building Code Requirements for Structural Concrete Reinforced with Glass-Fiber Reinforced Polymer (GFRP) Bars - Code and Commentary. American Concrete Institute, United States of America.

ACI 440.1R-15 (2015). Guide for the Design and Construction of Structural Concrete Reinforced with Fiber-Reinforced Polymer (FRP) Bars. American Concrete Institute, United States of America.

Al-Mayah, A., Soudki, K. and Plumtree, A. (2006). Development and assessment of a new CFRP rod-anchor system for prestressed concrete. Applied Composite Materials 13: 321–334. https://doi.org/10.1007/s10443-006-9019-6.

Alraie, A. and Matsagar, V. (2023). Flexural performance of basalt fiber-reinforced polymer prestressed concrete beams. ACI Structural Journal 120: 187–202. https://doi.org/10.14359/51736123.

ASTM D7205/D7205M-21, A. (2021). Standard Test Method for Tensile Properties of Fiber Reinforced Polymer Matrix Composite Bar. American Society for Testing and Materials, United States of America.

Atutis, M., Valivonis, J. and Atutis, E. (2015). Analysis of serviceability limite state of GFRP prestressed concrete beams. Composite Structures 134: 450–459. https://doi.org/10.1016/j.compstruct.2015.08.062.

Cagnoni, A., Colombi, P., Pisani, M.A. and D'Antino, T. (2024). Effectiveness of FRP bar anchors for prestressed concrete members. Procedia Structural Integrity 64: 944–950. https://doi.org/10.1016/j.prostr.2024.09.374.

Esmaeili, Y., Mohamed, K., Newhook, J. and Benmokrane, B. (2021). Assessment of creep rupture and long-term performance of GFRP bars subjected to different environmental exposure conditions under high sustained loads. Construction and Building Materials 300: 1–12. https://doi.org/10.1016/j.conbuildmat.2021.124327.

fib Model Code for Concrete Structures 2020 (2024). The International Federation for Structural Concrete, Switzerland.

Gu, X. and Ansari, F. (2000). Bond strength and strain distribution in the anchorage zone of post-tensioned CFRP tendons. Condition Monitoring of Materials and Structures: 120–133. https://doi.org/10.1061/40495(302)10.

Heo, S., Shin, S. and Lee, C. (2013). Flexural behavior of concrete beams internally prestressed with unbonded carbon-fiber-reinforced polymer tendons. Journal of Composites for Construction 17: 167–175. https://doi.org/10.1061/(ASCE)CC.1943-5614.0000306.

Jeong, Y., Kim, W.S., Gribniak, V. and Hui, D. (2019). Fatigue behavior of concrete beams prestressed with partially bonded CFRP bars subjected to cyclic loads. Materials 12: 1-18. https://doi.org/10.3390/ma12203352.

Jiang, Z., Zhang, B., Zhao, C., Zhao, J., Lu, Z., Fang, J. and Xie, J. (2025). Long-term shear performance of prestressed GFRP bars in accelerated seawater aging: Role of alkalinity reduction in concrete matrix. Construction and Building Materials 463: 1–14. https://doi.org/10.1016/j.conbuildmat.2025.140039.

Le, T.D., Pham, T.M., Hao, H. and Hao, Y. (2018). Flexural behavior of precast segmental concrete beams internally prestressed with unbonded CFRP tendons under four-point loading. Engineering Structures 168: 371–383. https://doi.org/10.1016/j.engstruct.2018.04.068.

Le, T.D., Pham, T.M., Hao, H. and Yuan, C. (2019). Performance of precast segmental concrete beams with carbon fiber-reinforced polymer (CFRP) tendons. Composite Structures 208: 56–69. https://doi.org/10.1016/j.compstruct.2018.10.015.

Liang, Y., Sun, C. and Ansari, F. (2011). Damage assessment and ductility evaluation of post tensioned beams with hybrid FRP tendons. Journal of Composites for Construction 15: 274–283. https://doi.org/10.1061/(ASCE)CC.1943-5614.000016.

Lignola, G.P., Di Ludovico, M., Prota, A. and Manfredi, G. (2012). FRP Prestressed Concrete Structures. In: Nicolais, L. and Borzacchiello, A. (Eds.). Wiley Encyclopedia of Composites. 2nd ed. John Wiley & Sons. https://doi.org/10.1002/9781118097298.weoc218.

Lou, T. and Karavasilis, T.L. (2018). Time-dependent assessment and deflection prediction of prestressed concrete beams with unbonded CFRP tendons. Composite Structures 194: 365–376. https://doi.org/10.1016/j.compstruct.2018.04.013.

Lou, T., Lopes, S.M.R. and Lopes, A. V. (2016). Response of continuous concrete beams internally prestressed with unbonded FRP and steel tendons. Composite Structures 154: 92–105. http://dx.doi.org/10.1016/j.compstruct.2016.07.028.

Pincheira, J.A. and Woyak, J.P. (2001). Anchorage of carbon fiber reinforced polymer (CFRP) tendons using cold-swaged sleeve. PCI Journal 46: 100–111. https://doi.org/10.15554/pcij.11012001.100.111.

Poudel, P., Belarbi, A., Gencturk, B. and Dawood, M. (2022). Flexural behavior of full-scale, carbon-fiber-reinfoced polymer prestressed concrete beams. PCI Journal 67: 22–39. https://doi.org/10.15554/pcij67.5-01.

Rossini, M. and Nanni, A. (2019). Composite strands for prestressed concrete: State-of-the-practice and experimental investigation into mild prestressing with GFRP. Construction and Building Materials 205: 486–498. https://doi.org/10.1016/j.conbuildmat.2019.02.045.

Rossini, M., Saqan, E. and Nanni, A. (2019). Prediction of the creep rupture strength of GFRP bars. Construction and Building Materials 227: 1–11. https://doi.org/10.1016/j.conbuildmat.2019.08.001.

Shi, J., Wang, X., Wu, Z. and Zhu, Z. (2015). Relaxation behavior of BFRP tendon for presstressing application. In: Fernando, D., Teng, J.-G. and Torero, J.L. (Eds.). Proceedings of the Second International Conference on Performance-Based and Life-Cycle Structural Engineering (PSLE 2015). https://doi.org/10.14264/uql.2016.1109.

Wang, X., Xu, P., Wu, Z. and Shi, J. (2015). A novel anchor method for multi-tendon FRP cable: Concept and FE study. Composite Structures 120: 552–564. https://doi.org/10.1016/j.compstruct.2014.10.024.

Wang, Z., Xie, J., Li, J., Liu, P., Shi, C. and Lu, Z. (2022). Flexural behaviour of seawater–sea sand concrete beams reinforced with GFRP bars: Effects of the reinforcement ratio, stirrup ratio, shear span ratio and prestress level. Journal of Building Engineering 54: 1–21. https://doi.org/10.1016/j.jobe.2022.104566.

Wolff, R. and Miesseler, H.-J. (1993). Glass fibre prestressing system. In: Nanni, A. (Ed.). Fiber-Reinfoced-Plastics (FRP) Reinforcement for Concrete Structures: Properties and Applications. Elsevier.

Wu, J., Xian, G. and Li, H. (2018). A novel anchorage system for CFRP cable: Experimental and numerical investigation. Composite Structures 194: 555–563. https://doi.org/10.1016/j.compstruct.2018.04.006.

Younes, T., Al-Mayah, A. and Topper, T. (2017). Fatigue performance of prestressed concrete beams using BFRP bars. Construction and Building Materials 157: 313–321. https://doi.org/10.1016/j.conbuildmat.2017.09.086.

Zawam, M., Soudki, K. and West, J.S. (2017). Effect of Prestressing Level on the Time-Dependent Behavior of GFRP Prestressed Concrete Beams. Journal of Composites for Construction 21: 1–10. https://doi.org/10.1061/(ASCE)CC.1943-5614.0000783.

Zhao, J., Mei, K. and Wu, J. (2020). Long-term mechanical properties of FRP tendon–anchor systems — A review. Construction and Building Materials 230: 1–15. https://doi.org/10.1016/j.conbuildmat.2019.117017.

Appendix A

In this section, the concrete stresses at specific points on the cross-section of a beam with two prestressed GFRP bars are calculated. Prestress losses are neglected in this analysis. As the prestressing forces are not applied within any plane of symmetry of the cross-section, the eccentricities in both principal directions are taken into account. According to Saint Venant's principle, the original load (a compressive force acting on the concrete) can be replaced by an equivalent system consisting of a force P and two bending moments, Mx and My, applied at the centroid of the cross-section. Figure A.1 illustrates the beam cross-section with both the original and the equivalent loading systems. The prestressing force is applied to one bar at a time.

Normal stresses were calculated at points A, B, C, and D, which define the corners of the rectangular cross-section of the beam. These stresses were determined using Equation 1, where the first term corresponds to the prestressing force, the second to the bending moment Mx, and the third to the bending moment My. The normal stresses induced by Mx and My vary linearly across the section. Points E and F correspond to the locations where strain gauges were installed to monitor strains.

$$\sigma = \frac{P}{A} \pm \frac{P \quad e_y}{W_x} \pm \frac{P \quad e_x}{W_y} \tag{1}$$

where P is the applied prestressing force (kN); A is the cross-sectional area (m^2); e_x and e_y are the eccentricities in the x- and y-axis directions (m); and W_x and W_y are the section moduli about the x- and y-axes (m^3), as defined in Equations 2 and 3. The cross-sectional area is 0.039 m^2. The section moduli in the x- and y-directions are 1.69 × 10^{-3} m^3 and 9.75 × 10^{-3} m^3, respectively.

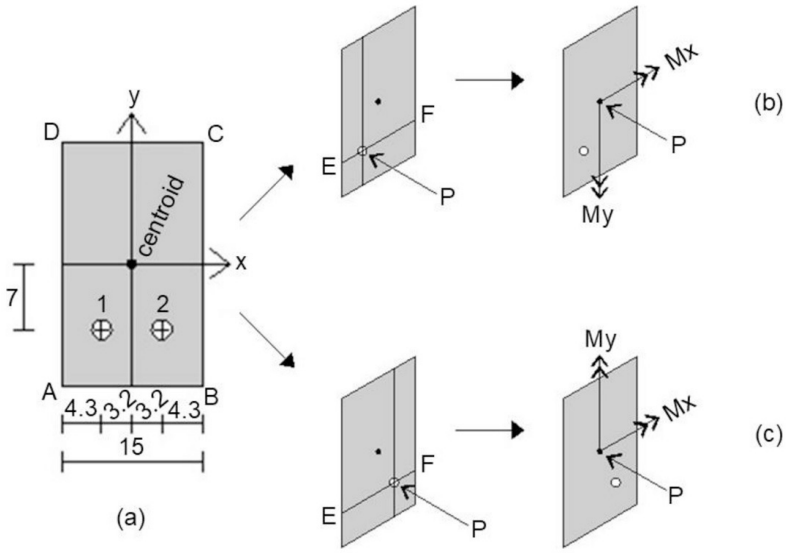

Figure A.1 Cross-section of a beam with two prestressed GFRP bars: (a) beam cross-section; (b) prestressing of the first GFRP bar, showing the original load and the equivalent static loading; (c) prestressing of the second GFRP bar, showing the original load and the equivalent static loading.

$$W_x = \frac{bh^2}{6} \tag{2}$$

$$W_y = \frac{\mathrm{hb}^2}{6} \tag{3}$$

where b and h denote the width and height, respectively, of the rectangular concrete cross-section shown in Figure A.1. The cross-section has a width of 15 cm and a height of 26 cm.

The calculated stresses at the four corners of the rectangular section are presented in Tables A.1 and A.2. Table A.1 corresponds to a prestressing force of 39.2 kN applied to each GFRP bar, while Table A.2 corresponds to a force of 24 kN applied to each bar. The tables also present the stresses at points E and F, calculated on the basis of the linear variation of stresses across the section due to bending moments Mx and My.

Table A.1 Concrete stresses induced by a 39.2 kN prestressing force applied to each GFRP bar in a beam containing two prestressed bars.

Stress distribution (MPa) induced by prestressing in the first GFRP bar						
Loading	Points					
	A	B	C	D	E	F
P	-1.01	-1.01	-1.01	-1.01	-1.01	-1.01
Mx	-1.62	-1.62	+1.62	+1.62	-0.87	-0.87
My	-1.29	+1.29	+1.29	-1.29	-1.29	+1.29
total	-3.92	-1.34	+1.91	-0.67	-3.17	-0.59
Stress distribution (MPa) induced by prestressing in the second GFRP bar						
Loading	Points					
	A	B	C	D	E	F
P	-1.01	-1.01	-1.01	-1.01	-1.01	-1.01
Mx	-1.62	-1.62	+1.62	+1.62	-0.87	-0.87
My	+1.29	-1.29	-1.29	+1.29	+1.29	-1.29
total	-1.34	-3.92	-0.67	+1.91	-0.59	-3.17
Total stresses (MPa) induced by the prestressing of both GFRP bars						
	Points					
	A	B	C	D	E	F
total	-5.26	-5.26	+1.24	+1.24	-3.76	-3.76

*The section details and positions of points A, B, C, D, E, and F are shown in Figure A.1.

Table A.2 Concrete stresses induced by a 24.0 kN prestressing force applied to each GFRP bar in a beam containing two prestressed bars.

Stress distribution (MPa) induced by prestressing in the first GFRP bar						
Loading	Points					
	A	B	C	D	E	F
P	-0.62	-0.62	-0.62	-0.62	-0.62	-0.62
Mx	-0.99	-0.99	+0.99	+0.99	-0.53	-0.53
My	-0.79	+0.79	+0.79	-0.79	-0.79	+0.79
total	-2.40	-0.82	+1.17	-0.41	-1.94	-0.36
Stress distribution (MPa) induced by prestressing in the second GFRP bar						
Loading	Points					
	A	B	C	D	E	F
P	-0.62	-0.62	-0.62	-0.62	-0.62	-0.62
Mx	-0.99	-0.99	+0.99	+0.99	-0.53	-0.53
My	+0.79	-0.79	-0.79	+0.79	+0.79	-0.79
total	-0.82	-2.40	-0.41	+1.17	-0.36	-1.94
Total stresses (MPa) induced by the prestressing of both GFRP bars						
	Points					
	A	B	C	D	E	F
total	-3.22	-3.22	+0.76	+0.76	-2.30	-2.30

*The section details and positions of points A, B, C, D, E, and F are shown in Figure A.1.